Femtosecond laser texturing as a tool to increase the hydrophobicity of ornamental stone: The influence of lithology and texture

A.J. López, J.S. Pozo-Antonio, A. Moreno, T. Rivas, D. Pereira, A. Ramil

Journal of Building Engineering
https://doi.org/10.1016/j.jobe.2022.104176

Journal of Building Engineering 51 (2022) 104176

Contents lists available at ScienceDirect

Journal of Building Engineering

journal homepage: www.elsevier.com/locate/jobe

Femtosecond laser texturing as a tool to increase the hydrophobicity of ornamental stone: The influence of lithology and texture

A.J. López [a,*], J.S. Pozo-Antonio [b], A. Moreno [a], T. Rivas [b], D. Pereira [c], A. Ramil [a]

[a] Laboratorio de Aplicacións Industriais do Láser, Centro de Investigacións Tecnolóxicas, Universidade da Coruña, 15471, Ferrol, Spain
[b] CINTECX, GESSMin Group, Departamento de Enxeñaría de Recursos Naturais e Medio Ambiente, Escola de Enxeñaría de Minas e Enerxía, Universidade de Vigo, 36310, Vigo, Spain
[c] Department of Geology, Universidad de Salamanca, 37008, Salamanca, Spain

ARTICLE INFO

Keywords:
Femtosecond laser texturing
Wettability
Hydrophobicity
Ornamental stone

ABSTRACT

In the field of stone conservation, a very common direct intervention seeks to increase the water repellence of objects. By limiting the interaction between the solid and the water, the possibility of alteration due to the action of the water (liquid or solid) as well as that related to the colonisation of surfaces by organisms is reduced. To decrease wettability, chemicals are often applied to create a surface layer; however, laser texturing, currently used in different industrial and technological fields, could be considered as an alternative procedure, thus eliminating exposure to chemicals with varying degrees of toxicity. In this paper, modification of the wetting properties of stone surfaces upon texturing induced by a femtosecond laser structuring process was investigated. Four ornamental stones with different mineralogic and chemical compositions (slate, quartzite, granite and marble) and other surface characteristics were laser processed by applying different texturing patterns (parallel grooves and matrices of craters) and different irradiation parameters. After texturing, variations on the wettability characteristics of the different rock surfaces were evaluated by means of static contact angle measurements and modifications on the topography were studied via confocal microscopy. Furthermore, potential harmful effects on the ornamental stones were evaluated through colour spectrophotometry, petrographic microscopy and SEM-EDX. The results indicate two different behaviours in the ornamental stones analysed that were statistically confirmed: on the one hand, the group formed by slate, quartzite and granite, in which the laser texturing caused a decrease in the contact angle and, on the other hand, marble in which laser texturing was able to increase the contact angle above 90°, giving the stone surface a hydrophobic character. The topographic analyses together with microscopy observations indicate that the grain size, mineral composition, type of fissures and initial surface quality of the stones were key in the different wetting behaviour of the laser textured stones.

1. Introduction

Water repellents are commonly used in outdoor architectural heritage in order to reduce the interaction between materials and water [1], consequently reducing physical and chemical modifications in the materials related to the action of water (hydrolysis,

* Corresponding author.
E-mail address: ana.xesus.lopez@udc.es (A.J. López).

https://doi.org/10.1016/j.jobe.2022.104176
Received 8 November 2021; Received in revised form 4 February 2022; Accepted 4 February 2022
Available online 1 March 2022

complexation, dissolution, ice-taw stress) and to the metabolism of colonising organisms [2,3]. Hydrophobic surfaces demonstrate a notable advantage in outdoor conditions, mitigating undesirable effects (such as colour changes or the growth of microorganisms) due to the penetration of water generated by condensation [4–6].

Today, compounds that modify the wettability characteristics of a solid surface are attracting a lot of attention. In this sense, polymeric resins are usually applied to stone monuments as protective hydrophobic coatings [7,8]; their application by brush or spray onto a stone surface creates a coating that confers micro-and nano-hierarchical roughness, which contributes to enhancing the hydrophobicity of the solid [9–11], simulating the hydrophobic properties found in nature [12,13]. This micro-nano binary roughness can be obtained by adding inorganic nanoparticles (silica, aluminium, tin and titanium oxides) to polymers (generally siloxanes) [6,14,15] with the possible addition of surfactants (n-octylamine) and/or organosiloxanes (polymethylsiloxane-PDMS) [16,17].

In general, water repellents show several drawbacks as products obtained in the chemical industry: i) they usually contain substances that are toxic to human health and ii) they can constitute environmental hazards. Moreover, like almost all chemicals applied to consolidate, clean or protect stones, water repellents can cause side effects, such as colour changes or a modification in water transport through the stone, which can reduce compatibility with the material to be treated [18].

Surface structuring by laser processing, both in nanosecond (ns) and femtosecond (fs) pulse regimes, has been widely applied to modify the wettability and other surficial properties of different materials like polymers, semiconductors or metals, among others [19,20]. Short (ns regime) laser pulses present much larger thermal effects than ultra-short (fs regime) lasers, resulting in large heat-affected zones, debris and remelting in the processed area, and consequently less precision and accuracy than ultrafast (fs) laser structuring [21–23].

Regarding stones, in general, very little research has been reported on laser structuring as an alternative for modifying wettability. A nanosecond pulse laser was used to structure a commercial variety of Zimbabwe black granite (a medium-to fine-grained gabbro) to increase hydrophobicity [24,25], and, to the best of our knowledge, our group was the first to apply an ultra-short (femtosecond) laser for texturing ornamental stones [26]. In that pioneering work, hydrophobicity of a pure marble (Crystal White) was induced by femtosecond laser structuring and, in some cases, nearing super-hydrophobic behaviour was obtained. Recently [27], a short and long-term evolution of the wettability characteristics of marble upon ultrafast laser texturing was investigated in order to elucidate the combined effect of multi-scale roughness and the attachment of chemical species at the surface over time.

However, due to the versatility of the femtosecond laser structuring process, research elucidating correlations between the surface topography generated and wetting response of laser-structured materials is still being intensely investigated [28]. These studies are essential in the case of materials, such as natural stone, in which the challenge is their heterogeneity that causes different interaction mechanisms of the laser pulses with each type of grain, leading to irregular surface absorption [29].

In the research described in this article, for the first time, it was accomplished a comparative analysis of the modification, through femtosecond laser texturing process, of the wetting characteristics of four ornamental stones commonly used in architectural cultural heritage worldwide (slate, quartzite, granite, and marble). This work has two main objectives: 1) to research the effectiveness of femtosecond laser structuring process to attain the hydrophobicity as a function of i) the lithology and the superficial characteristics of the four ornamental stones and ii) the texturing conditions (type, periodicity, and size of the structures generated); and 2) to research the adverse effects on the physical properties of the stones (i.e. colour) and the stability of the composing minerals through petrographic microscopy and scanning electron microscopy.

2. Contact angle and wetting phenomena

When a drop of liquid is set upon a solid's flat surface, a system of three interfaces is generated; a liquid-vapour a solid-liquid, and a solid-vapour interface. The wetting behaviour of a solid surface is driven by the surface free energy at these interfaces, and the contact angle θ of the liquid drop with the surface is the main index used to evaluate the wettability of a solid surface [30]. The contact angle is defined as the angle between the tangent at three phase point and the solid surface, and it is the key aspect in determining the shape of the liquid drop. In ideal systems in which the solid surface is smooth, homogeneous, and rigid the Young contact angle θ_0 characterizes the equilibrium state of the solid−liquid−vapour. The situation is quite different in real systems because nearly all solid surfaces are rough and chemically heterogeneous to some extent. This implies that θ_0 is in general not equal to the contact angle measured in an experiment.

On rough surfaces, equilibrium wetting is discussed in terms of the 'competition' between complete liquid penetration into roughness grooves or holes and the entrapment of air bubbles inside these grooves underneath the liquid. The former is the homogeneous wetting regime, usually described by the Wenzel model, while the latter is the heterogeneous wetting regime described by the Cassie-Baxter model [31]. The Wenzel equation (Eq. (1)) yields the Wenzel apparent contact angle θ_W as a function of the Young contact angle θ_0 and the roughness ratio r that is defined as the ratio of the actual surface area wetted by the liquid and the projected planar area $(r > 1)$.

$$\cos\theta_W = r\cos\theta_0 \tag{1}$$

Wenzel equation (Eq. (1)) is based on the hypothesis that liquid enters grooves or holes present on the surface, leading to a homogeneous wetting regime with an increased contact area. This model explains why the contact angle of hydrophilic surfaces ($\theta_0 < 90°$) decreases with increasing roughness whereas the contact angle of hydrophobic surfaces ($\theta_0 > 90°$) increases.

In the heterogeneous wetting regime given by the Cassie-Baxter model (Eq. (2)), the surface tension dominates the system and is energetically favourable for the liquid to form a droplet that rests on the edges of the surface while air fills the space between solid and liquid, forming air pockets. Consequently, only a small fraction of the solid surface is in contact with the liquid. The Cassie-Baxter

contact angle θ_{CB} can be calculated as:

$$\cos\theta_{CB} = -1 + f + r_f f \cos\theta_0 \quad (2)$$

where f is the fraction of the projected area of the solid surface under the drop that is wetted by the liquid and r_f is the roughness ratio of the wetted area. When $f = 1$, $r_f = r$ and the Cassie-Baxter equation is equivalent to the Wenzel equation. Therefore, for a given surface composition and liquid, i.e. by fixing θ_0, the nature of the texture determines the wetting behaviour. It is important to note that both equations are correct only if the drop is sufficiently large in relation to the typical roughness scale [32].

3. Materials and methods

3.1. Ornamental stones

Four different lithologies were selected: a slate, a quartzite, a granite, and a marble (Fig. 1, a-d, respectively). All of them were provided by a stone company and we specify the commercial names when available.

The slate (Fig. 1a) selected is from the Luarca slate geologic formation from the Ordovician period (435–500 mya), which is a monotonous succession of black and grey slates with collations of coarse detrital levels [33]. The sample corresponds to the highest quality facies used as roofing slate, characterised by a very fine grain, a very homogeneous texture, high fissility, and a lower content of metallic sulphides. Its porosity accessible to water (in accordance with UNE EN 1936:2006 [34]) is 0.8%. The selected quartzite (Fig. 1b) goes by the trade name *Perla Venata* and is mined in Brazil. Its pale cream colour with brownish tonalities, associated with the presence of fine sand veining, combined with its hardness and low open porosity (0.97% according to the product information sheet) make this material a highly appreciated ornamental stone both for interiors and facade cladding. The granite (Fig. 1c) goes by trade name *Vilachán* and is quarried in NW Spain. It is a fine-grained panallotriomorphic heterogranular ademellite with an open porosity of

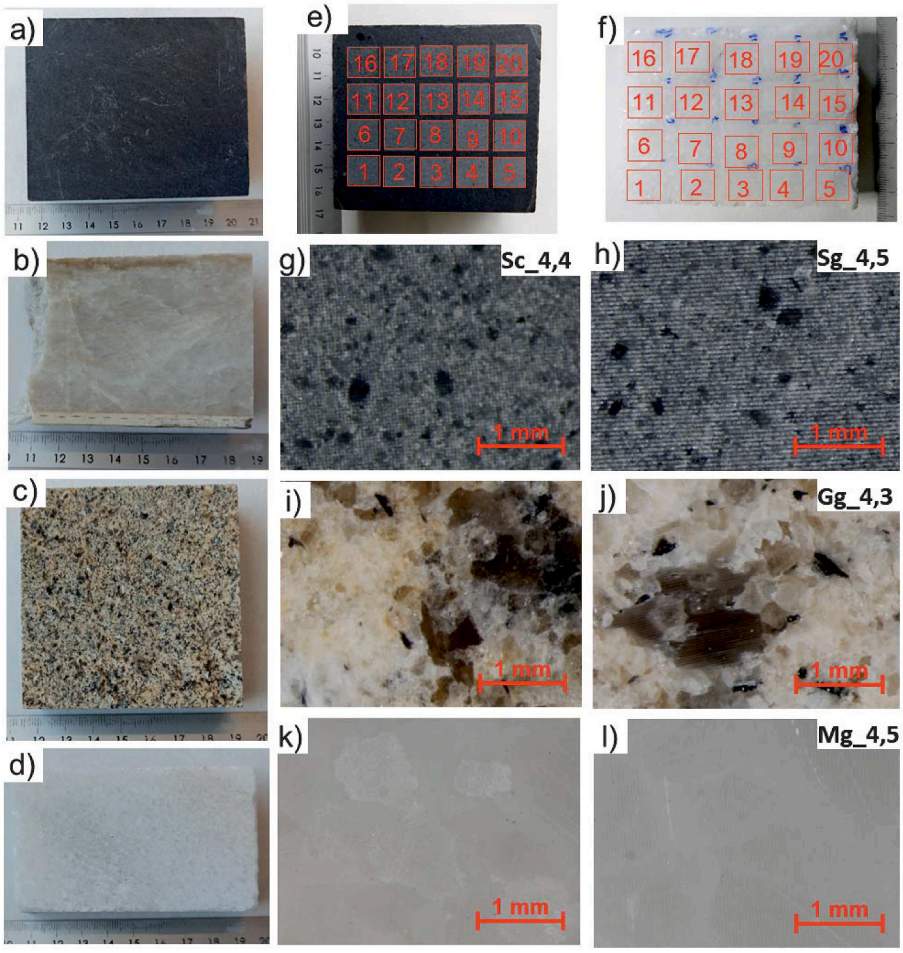

Fig. 1. a-d) images of the four selected stones: a) slate, b) quartzite, c) granite, and d) marble; e-f) slate and marble slabs after laser texturing, respectively, indicating the 20 textured areas; g-h) micrographs taken via stereomicroscopy of the slate slabs textured with craters (g) and grooves (h); i-j) micrographs taken via stereomicroscopy of the untextured granite slab (i) and an area textured with grooves (j); k-l) micrographs taken via stereomicroscopy of the untextured marble slab (k) and an area textured with grooves (l). The images shown contain the ID of the textured area.

2.82% [35]. Finally, the selected marble (Fig. 1d) is the stone commercially known as *Crystal White*, a Vietnamese white-coloured pure marble with an equigranular and fine-grained texture. Its open porosity is 0.01% [34].

Therefore, 3 slabs of each stone measuring approximately 10 cm × 5 cm x 2 cm were polished and their surfaces were cut (Fig. 1, a-d). Two slabs were sent for laser texturing and the third one was used as an untreated reference stone.

3.2. Laser texturing

Laser texturing experiments were performed by means of a computer-controlled galvanometer- and scanner-equipped femtosecond pulsed near-infrared laser, and specifically the Spirit system by Spectra-Physics, with an emission wavelength of 1040 nm and pulse width of less than 400 fs, as previously used for texturing purposes [26]. The intensity profile at the laser output was near-Gaussian ($M^2 < 1.2$) and the diameter of the beam was 1.5 mm with horizontal polarisation (>100:1). The pulse rate can be set from a single shot to 1 MHz, with a maximum pulse energy of 40 μJ at 100 kHz. The maximum mean power output is > 4 W. A two-mirror galvanometric scanner (Raylase SuperscanIII-15) scans the laser beam on the X- and Y-axes. In this experiment, the beam was focused via an F-theta objective lens with a focal length of 160 mm, up to a diameter of 30 μm. In the working plane, the beam polarisation is parallel to the Y-axis. Laser surface treatments were performed in the air at atmospheric pressure.

During the preliminary testing, we determined the parameters most suitable for obtaining uniform textures with similar dimensions across the different stones. Once the most suitable parameters for each stone were selected, two types of patterns were generated: a matrix of crater-like holes and arrays of parallel grooves. Crater-like holes were obtained through successive laser shots delivered at the same point in the surface while grooves were obtained via overlapping holes as the laser beam scanned along the X- or Y-axis.

To analyse the relationship between the texture generated on the stones' surfaces and its effect on their wettability, patterns with different geometric features (periodicity and pattern depth) were tested, varying the pitch between the structures generated (craters or grooves) and the laser power applied. For each stone, the frequency, scan velocity (in grooves) and number of laser shots (in holes) remained the same. As mentioned above, this was done in order to obtain similar texturing patterns independent of the type of stone. Four laser power values were applied, ranging from 100% of maximum power (4 W) to 40% of maximum power (1.6 W), along with 5 different pitch distances. The irradiation conditions are given inTable 1.

In total, for each stone, 20 sections measuring 1 × 1 cm^2 were textured with grooves (using one slab; see Fig. 1e) and another 20 sections measuring 1 × 1 cm^2 were textured with craters (a second slab was used; see Fig. 1f).

Each textured area was identified with a letter indicating the stone (slate-S, quartzite-Q, granite-G, and marble-M), the texture pattern (g-grooves, c-crater), the power (from 4 (max.) to 1 (min.)) and the pitch (8 for 80, 7 for 70, etc). For example, Mg_4,5 refers to groove-textured marble at maximum power (4 W) with a pitch distance of 50 μm.

3.3. Analysis techniques

3.3.1. Ornamental stone characterisation

For this study, the geochemical, petrographic, and mineralogical characterisation of the stone samples was performed. The chemical composition (whole-stone major and trace elements) was obtained by means of inductively coupled plasma mass spectrometry (ICP-MS) using an ICP-MS AGILENT 7800. For the analysis, 0.1 g of sample powder was digested with HNO_3 + HF under pressure in high pressure vessels in a Milestone microwave.

Qualitatively, the mineralogical composition was obtained via the X-ray powder diffraction analysis (Bruker D8 Advance) of bulk stone with CuKα radiation and a velocity of 2θ/min. The equipment used was a Siemens D-500 (40 kV and 30 mA) diffractometer using a CuKα radiation (λ = 0.15437 nm) Ni-filter, equipped with the Diffract ATV3 software package.

A complete petrographic examination was done following standard ASTM C1721-15 [36] in order to describe the mineralogy and textures. A Leica DM2500P microscope under transmitted light was used for this purpose.

3.3.2. Wettability evaluation and laser texture characterisation

To evaluate the wettability of the textured surfaces, the static contact angle θ was measured with a Phoenix-300 equipped with an automatic dosage system and a 6.5x zoom CCD camera. For each textured area and for the reference surfaces, the static contact angles of three 4 μL droplets were measured, with a precision of ±0.1°, following the sessile drop method indicated in Standard EN 828:2013 [37].

The characterisation of the surface texture was carried out with a Sensofar Plu 2300 confocal microscope with an XY motorised

Table 1
Laser processing parameter values: mean power, repetition frequency, pattern pitch, scan speed (grooves), and irradiation time (holes) for each of the stones (S: slate, Q: quartzite, G: granite, and M: marble) textured with grooves (g) and craters (c).

Sample	power [W]	freq. [kHz]	pitch [μm]	speed [mm/s]	time [ms]
Sg	1.6, 2.4, 3.2, 4.0	2	40, 50, 60, 70, 80	2.5	
Sc	1.6, 2.4, 3.2, 4.0	2	40, 50, 60, 70, 80		16
Qg	1.6, 2.4, 3.2, 4.0	20	20, 30, 40, 50, 60	10	
Qc	1.6, 2.4, 3.2, 4.0	20	20, 30, 40, 50, 60		6.25
Gg	1.6, 2.4, 3.2, 4.0	20	30, 40, 50, 60, 70	10	
Gc	1.6, 2.4, 3.2, 4.0	20	30, 40, 50, 60, 70		6.25
Mg	1.6, 2.4, 3.2, 4.0	50	20, 30, 40, 50, 60	20	
Mc	1.6, 2.4, 3.2, 4.0	50	20, 30, 40, 50, 60		5

stage and using a 20× EPI objective (field of view: 637 μm × 477 μm, resolution: 768 pixels × 576 pixels, Z-scan resolution: 0.1 μm). Data processing, analysis, and display were carried out using ScientificPython. Two different analyses were carried out using the topographies of the different tests:

1) Determination of the parameters related to the analysis of 3D areal surface texture in accordance with standard UNE-EN ISO 25178-2 [38]: S_a, the mean roughness; S_q, the root mean square value of the ordinate values; S_{sk}, the skewness of the scale-limited surface; S_{ku}, the kurtosis of the scale-limited surface; and S_{dr}, the developed interfacial area ratio, which is a hybrid parameter expressed as the percentage of the definition area's additional surface area contributed by the texture compared to the planar definition area. This parameter is directly related to parameter r in Wentzel's equation (Eq. (1)), given that $r = 1 + S_{dr}$.
2) Fitting the confocal topographies to a periodic succession of Gaussians in order to obtain the average values of the depth z_p and width w_p of the texture patterns. In the case of grooves, the average profile was fitted to a series of equally spaced Gaussians. In the case of craters, the surface was adjusted to a series of Gaussians distributed across a two-dimensional lattice. By doing so, we obtained the average depth and width values of the patterns, which are more significant than measuring a single groove or crater [39].

Furthermore, the reference and textured surfaces with the lowest and the highest static contact angles for each stone and pattern were observed using a stereomicroscope (SMZ 1000) and carefully cut in order to view them under scanning electron microscopy (SEM) with energy dispersive X-ray spectroscopy (EDS) using an FEI Quanta working in secondary electrons (SE) and backscattered electrons (BSE) modes. The optimum conditions of observation were obtained at an accelerating potential of 15–20 kV, a working distance of 9–11 mm, and a specimen current of 60 mA. Samples were C-coated. Moreover, to characterise the extent of the textured pattern in depth, these same samples were embedded in resin and cut perpendicularly to the textured surfaces, preparing both polished specimens and thin sections. The polished specimens were C-coated and viewed using SEM-EDS under the above-mentioned optimum conditions. Thin sections were viewed under transmitted light with a Leica DM2500P petrographic microscope, describing the mineralogy and textures following standard ASTM C1721-15 [36].

3.3.3. Effect on stone colour

Finally, variations in stone colour were analysed in order to evaluate the impact of the laser texturing on the rocks' properties as ornamental stones. Colour changes were evaluated by taking colorimetric measurements using a Minolta CM-700d spectrophotometer equipped with SpectraMagicTM Nx software. Colour was expressed in CIELAB and CIELCH spaces [40].

The parameters measured were the lightness (L*), which varies from black (0) to white (100); a*, which varies from +60 (red) to −60 (green); b*, which ranges from +60 (yellow) to −60 (blue); chroma (C^*_{ab}), which represents the saturation of the colour; and the hue (h_{ab}) or tone. Measurements of these parameters were done in Specular Component Excluded (SCE) mode with a spot diameter of 8 mm, illuminant D65, and an observer angle of 10°. A total of 9 measurements were taken for each surface in order to obtain statically representative results. Compared to the colour of the stone without texturing, the differences (ΔL^*, Δa^*, Δb^*, ΔC_{ab}^*, and ΔH^*) and the global colour change (ΔE^*_{ab}) were calculated [40].

3.3.4. Correlation relationships

In order to identify the relationships between texturing conditions (type of pattern, laser power and pitch) and the measured properties (contact angle, surface texture parameters, and colour), two statistical analyses were applied. To do so, the texturing conditions (power and pitch) were defined as predictor variables and the values of the contact angle θ, the surface texture parameters z_p and S_{dr}, and the global colour change ΔE^*_{ab} were defined as response variables.

First, a multiple regression analysis was performed to determine whether a change in the predictor variables was related to a change in the response variables. The p value of the null probability hypothesis was determined, that is, the probability that this linear regression is due to the randomness of the values. This p-value was determined for each one of the predictor variables and for the set of them. Linear relationships with probability values less than 5% (significance level of 0.05) were considered significant. In these cases, the value of the Pearson correlation coefficient R^2 was determined.

Second, a linear correlation analysis was performed between the response variables and the cosine of the contact angle to determine whether they followed the Wenzel or the Casie-Baxter model. The values of the null hypothesis probability p and the linear correlation coefficient R^2 were obtained.

4. Results

4.1. Ornamental stone characterisation

The slate is made up of phyllosilicates (muscovite, biotite, and chlorite, the latter as porphyrolasts, surrounded by foliation). Some quartz and plagioclase were also identified, along with accessories such as tourmaline and opaque minerals. The stone has a granoblastic-lepidoblastic texture. Quartz grains are elongated, following the foliation, creating pressure shadows, probably influencing the strength of the stone. The quartzite is made up of quartz and clay minerals. The stone has a granoblastic texture that is heavily deformed, with elongated quartz grains and multiple fractures filled with clay minerals. The Vilachán granite is a medium-grain granite composed of quartz, plagioclase, and potassium feldspar as its main mineral phases. Muscovite and biotite are the most important accessories (the first one is more abundant), along with cordierite, sillimanite, tourmaline, apatite, and zircon. The mineralogy does not show much alteration, except for some biotites that have partially transformed into chlorite. The granite has a conspicuous foliation, demonstrated by the orientation on micas. Crystal White marble is mainly composed of calcite, with a minimum

amount of dolomite. It contains 51.91% Ca (expressed as CaO) and has a loss on ignition of 42.60%. Under petrographic microscopy, the purity of the marble is confirmed as well as its mosaic, granoblastic texture, in which individual crystals of calcite meet others with somehow indented edges. Table 2 shows the chemical composition of the four stones.

4.2. Wettability and texturing characterisation

The values of the static contact angle θ of the four stones after texturing with grooves and craters, and for each of the irradiation conditions (power and pitch), are represented in Fig. 2.

The θ value of the non-textured stones is also shown (Fig. 2a: S-slate, 2b: Q-quartzite, 2c: G-granite and 2d: M-marble). Regarding the reference values, the four stones presented static contact angles below 90°. Slate, quartzite, and marble (Fig. 2a, b, 2d) have close values: $\theta_{slate} = 73.4° \pm 4.7°$, $\theta_{\text{quartizite}} = 69.7° \pm 0.6°$, and $\theta_{marble} = 66.2° \pm 5.8°$, however granite (Fig. 2c) had a lower value, $\theta_{granite} = 45.9° \pm 6.2°$. Note that these values correspond to stone surfaces subjected to a polished finish, which usually confers mild water-proofing properties. Polishing is a finishing procedure suitable for low porosity stones, such as slate, quartzite, and marble. However, the higher the porosity, the less the polishing effect. Therefore, the granite with the highest porosity showed the lowest θ value due to the reduced effectiveness of polishing.

After texturing, we observed that the contact angles of the slate, quartzite and granite (Fig. 2a, b, and 2c, respectively) decreased regardless of the type of pattern, power, and pitch, meaning that the texturing was unable to waterproof these surfaces. Conversely, in marble (Fig. 2d), the contact angle θ of all textured areas (except for Mg_1,6, Mg_1,5, and Mc_4,2) increased well above the reference value. In all textured areas of the marble, θ reached values above 90° with the exception of Mg_4,2, Mg_1,6, Mg_1,5, Mc_4,2, Mc_1,6, and Mc_1,4, with it consequently acquiring hydrophobic behaviour [9].

It is important to highlight the limited contact angle data obtained from the granite (Fig. 2c), which made it necessary to exclude this stone from the analysis. This happened because the drops of water lost balance on the surface of this stone and most of them broke as soon as they touched the surface. The difficulty in measuring θ lies in the granite's texture and, therefore, the limited effectiveness of polishing. The three typical granite fissures (inter-, intra-, and *trans*-granular fissures [41] make the droplets unstable once they come into contact with the surface.

As indicated in Section 2: Materials and Methods, the characterisation of textures was carried out based on confocal topographies, adjusting pattern profiles to Gaussian curves. An example of the reconstruction of the surface topography (500 μm × 600 μm) by adjusting to a series of Gaussians is shown in Fig. 3, which shows the results for a pattern of parallel grooves with a separation of 60 μm generated at the laser's maximum power of 4 W on samples of slate, quartzite, and marble as well as the different granite minerals. Topography data were used to obtain their dimensions (width w_p and depth z_p) as well as the different surface roughness parameters.

First, the average surface roughness values S_a were obtained for each polished stone prior to laser texturing in order to obtain a reference value for each stone. Specifically, slate had the highest average roughness at $S_a = 2.4$ μm, followed by granite at $S_a = 1.6$ μm, marble at $S_a = 0.25$ μm, and, lastly, quartzite at $S_a = 0.18$ μm. Nonetheless, it is necessary to keep in mind that these values were obtained from polished regions of the stones not containing irregularities (fissures, holes …) with dimensions much larger than the dimensions of the texturing. The surface roughness values obtained for all texturing conditions are included in Supplementary Data S1.

To characterise the laser-generated texture, first we focused on the depth z_p obtained by the structures, whether grooves or craters, given that the width is determined by the diameter of the laser beam and is therefore practically constant in all cases. The z_p values for the different stones and texturing patterns are given in Fig. 4.

Table 2
Chemical composition (major and selected trace elements) of the 4 stones obtained via ICP-MS. BDL: below detection limit; LOI: lost on ignition.

Compound	Slate	Quartzite	Granite	Marble
SiO2	73.03	95.34	75.36	4.43
TiO2 (%)	0.76	0.02	0.13	0.01
Al2O3 (%)	11.39	2.23	13.00	0.07
Na2O (%)	1.63	0.31	2.94	0.07
CaO (%)	0.50	0.11	0.57	51.91
K2O (%)	2.29	0.54	4.69	0.02
Fe2O3 (%)	5.67	0.46	1.56	0.10
MgO (%)	1.03	0.07	0.19	0.66
MnO (%)	0.07	0.01	0.01	0.02
P2O5 (%)	0.13	0.01	0.25	0.01
LOI (%)	3.50	0.90	1.30	42.7
Li (ppm)	99.8	3.5	343.32	1.1
Cr (ppm)	99.4	414.5	147.36	4.1
Co (ppm)	21.3	1.2	1.03	0.4
Cu (ppm)	29.4	10.4	8.73	8.6
Zn (ppm)	91.3	9.9	65.20	17.4
Rb (ppm)	25.4	18.4	370.31	0.3
Sr (ppm)	84.4	19.1	47.11	107.8
Zr (ppm)	178.6	52.8	74.17	4.0
Nb (ppm)	16.9	1.5	23.97	BDL
Ba (ppm)	331.0	24.2	144.17	4.0
Pb (ppm)	21.6	2.8	35.75	2.9

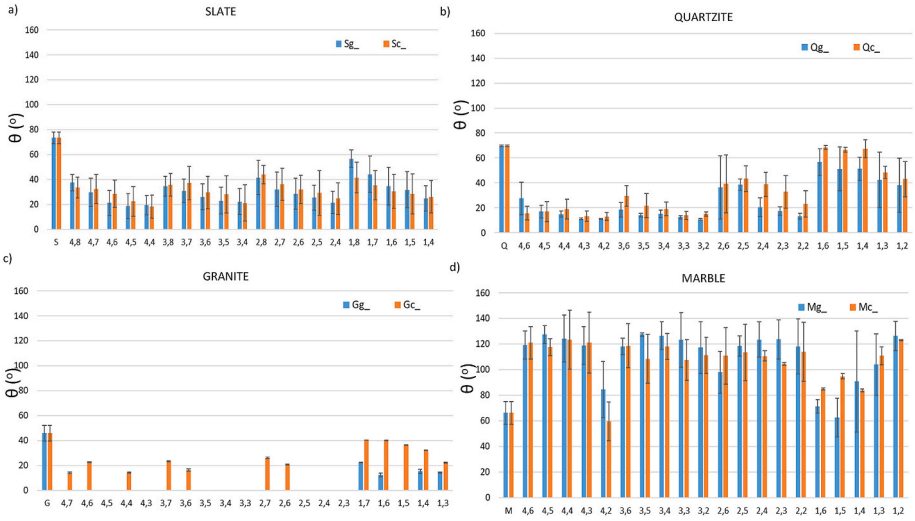

Fig. 2. Static contact angle θ measured by the sessile drop method (EN 828:2013) of the different textured areas: a) slate, b) quartzite, c) granite, and d) marble. Error bars length correspond to ± one standard deviation.

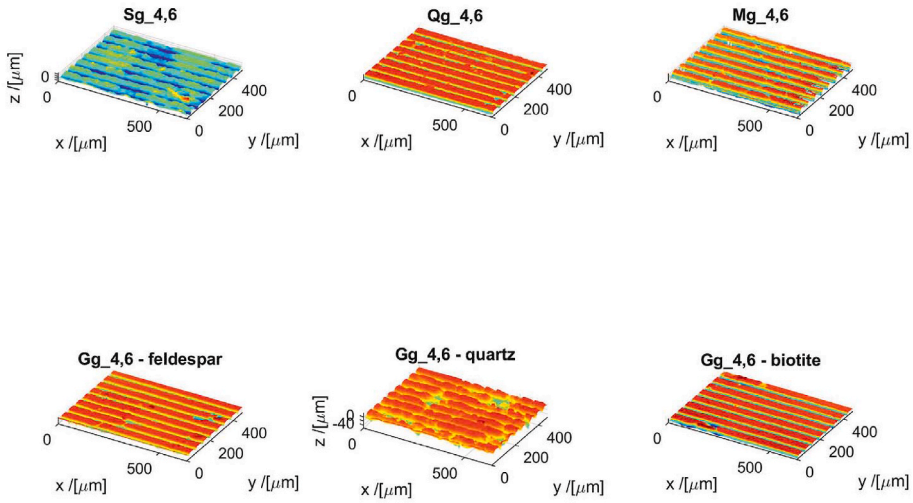

Fig. 3. Reconstruction of surface topography (500 × 600 μm) obtained by fitting the results of the confocal microscopy of a pattern of parallel grooves (pitch: 60 μm, power: 4 W) to a series of Gaussians, for the samples of slate, quartzite, marble, and the different granite minerals (quartz, feldspar, and biotite).

In all cases, we observe that the depth increases along with the power of the laser. Furthermore, we also observe – albeit not as clearly – that it increases along with the pitch, indicating that, at smaller spacings, the overlap of the laser shots reduces the height of the structures generated. This becomes evident in the case of the 20 μm separation in quartzite and marble. In general, the depth of the craters is greater than that of grooves since the laser shots are concentrated at specific points on the surface and not distributed along a line. In the case of granite, the values present a higher dispersion and higher error bars due to the presence of cracks and other defects in the polished surface. Roughness parameter that best approximates the increase in solid surface appearing both in the Wenzel and Cassie-Baxter models (Eq. (1) and Eq. (2), respectively) is S_{dr} (developed interfacial area ratio). The values of this parameter, also obtained via the confocal topographies, are shown in Fig. 5.

As observable, the general behaviour corresponds to an increase in S_{dr} with the use of the laser power and, conversely, a decrease in S_{dr} with its spacing. We also observed some higher values in the case of marble compared to the other stones. In general, the S_{dr} values in the groove-patterned surfaces are higher than those of the crater matrix pattern, contrary to what happened with depth z_p.

Table 3 presents the p values (null hypothesis probability) and Pearson correlation coefficient R^2 (in parentheses) of the multiple regression analysis of the relationship between the predictor variables (power and pitch) and the response variables (θ, z_p, S_{dr}, and ΔE^*_{ab}) for each of the stones textured with grooves and craters. Moreover, the p values for each response variable are shown along with the coefficient sign in parentheses.

First, Table 3 shows that there were no statistically significant differences between the values obtained with each texture pattern in

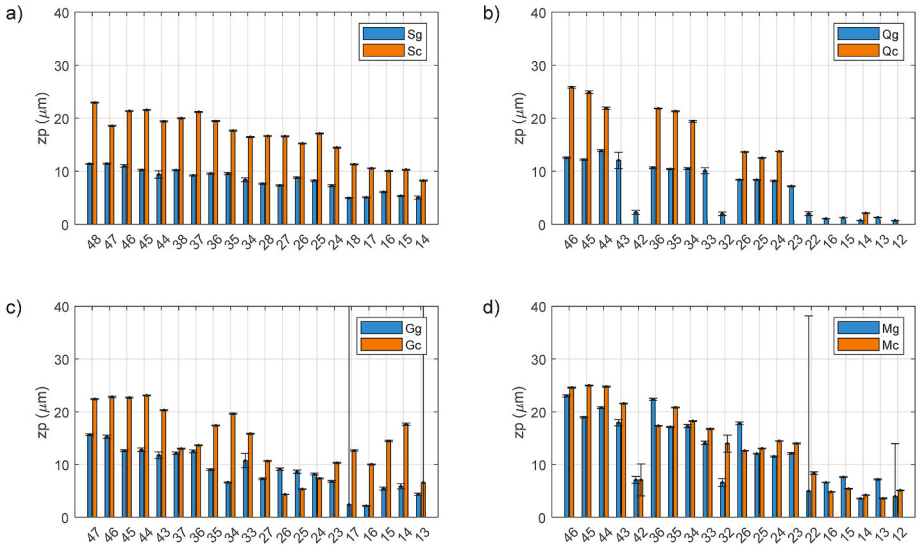

Fig. 4. Texture depth z_p obtained from the confocal topographies of the different rocks: a) slate, b) quartzite, c) granite, and d) marble. Error bars length correspond to ± one standard deviation..

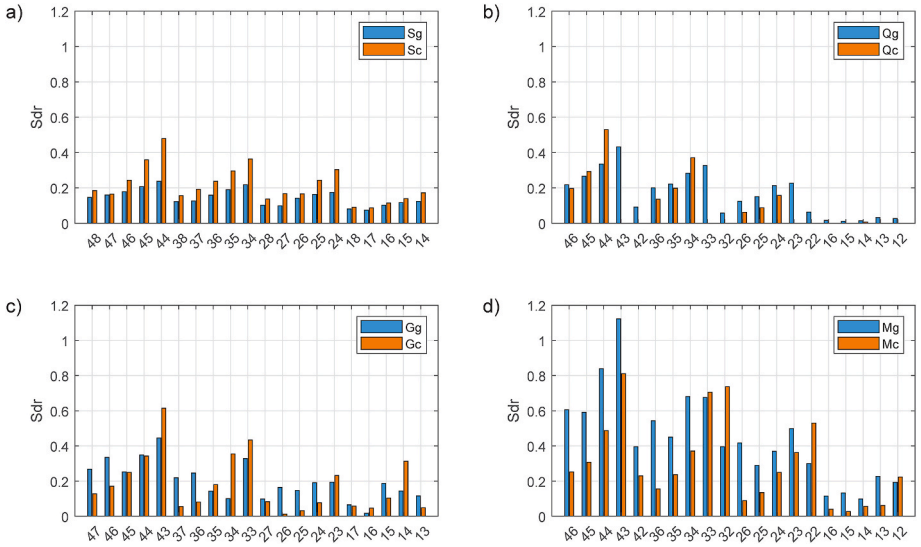

Fig. 5. Surface roughness S_{dr} (developed interfacial area ratio) obtained from the confocal topographies of the different rocks: a) slate, b) quartzite, c) granite, and d) marble.

any of the stones. However, within each texturing pattern, statistically significant differences were observed in the contact angle θ obtained at different power and pitch values. For slate and quartzite, in which θ decreased after texturing, we observed that 1) the greater the power, the smaller the θ (i.e., negative slope) and 2) the smaller the pitch, the smaller the θ (i.e., positive slope). These relationships were confirmed as being statistically significant by the statistical regression analysis.

Comparing the results obtained for slate and quartzite (Fig. 2a and b, respectively) shows that the texturing of the quartzite caused a greater reduction in the initial θ (note that the reference values were similar in both stones): for the groove-textured areas, in quartzite, in general terms, values of θ close to 10° were achieved after texturing; on the contrary, in slate, the lowest θ obtained after texturing was 18°.

Marble was the only stone in which texturing increased the contact angle above 90° under the majority of conditions. The lowest values were obtained at a power of 4 W and a pitch of 20 μm, as well as the power 1.6 W and all the pitches essayed. In this stone, there was no statistically significant linear regression relationship between the predictor variables (power and pitch) and the response variable θ (contact angle), as the P value p is greater than 1% (above 5%) and the correlation coefficient R^2 is close to zero. In the groove-textured marble, the condition under which the highest contact angle was achieved ($\theta = 127.5°$) was that used in Ms_4,5 (100%

Table 3
p and *R2* (in parentheses) values of the multiple regression analysis of the predictor variables (power and pitch) and response variables (θ, z_p, S_{dr} and ΔE^*_{ab}) for each of the stones (S: slate, Q: quartzite, M: marble) textured with grooves (Sg, Qg, and Mg) and craters (Sc, Qc, and Mc). The values of the Pearson correlation coefficient of each response variable are also shown, with the sign of the coefficient being included in parentheses. Statistically, non-significant regression relationships ($p > 0.05$) have been replaced by a hyphen.

Sample	RV	power	pitch	*p* (*R2*)
Sg	θ	4.2e-05 (−)	1.9e-07 (+)	7.5e-08 (0.85)
	z_p	3.3e-10 (+)	0.086 (+)	1.4e-09 (0.91)
	S_{dr}	5.4e-10 (+)	2.4e-09 (−)	2.4e-11 (0.94)
	ΔE^*_{ab}	0.00026 (+)	8.6e-05 (−)	1.2e-05 (0.74)
Sc	θ	0.00022 (−)	4.9e-10 (+)	9.1e-10 (0.91)
	z_p	4e-09 (+)	0.024 (+)	1.4e-08 (0.88)
	S_{dr}	6.6e-06 (+)	1.5e-06 (−)	1.3e-07 (0.84)
	ΔE^*_{ab}	2.3e-08 (+)	5.1e-15 (−)	8.6e-15 (0.98)
Qg	θ	3.1e-06 (−)	0.0032 (+)	3.3e-06 (0.77)
	z_p	3.6e-05 (+)	0.0074 (+)	3.4e-05 (0.70)
	S_{dr}	0.00028 (+)	–	0.0011 (0.55)
	ΔE^*_{ab}	2.2e-05 (−)	0.068 (+)	5.1e-05 (0.69)
Qc	θ	1e-08 (−)	0.0025 (+)	2.2e-08 (0.87)
	z_p	3.4e-05 (+)	–	6.6e-05 (0.94)
	S_{dr}	0.00025 (+)	0.0031 (−)	0.00047 (0.89)
	ΔE^*_{ab}	1.9e-05 (−)	0.0018 (+)	1.1e-05 (0.74)
Mg	θ	0.044 (+)	–	–
	z_p	6.5e-06 (+)	8.5e-05 (+)	1.2e-06 (0.80)
	S_{dr}	1.9e-05 (+)	–	8.1e-05 (0.67)
	ΔE^*_{ab}	–	0.0025 (−)	0.0081 (0.43)
Mc	θ	–	–	–
	z_p	1.5e-06 (+)	0.023 (+)	3.4e-06 (0.77)
	S_{dr}	0.0015 (+)	0.002 (−)	0.00028 (0.62)
	ΔE^*_{ab}	–	–	–

laser power, 50 μm pitch), whereas, in the crater-textured marble, the condition producing the highest contact angle ($\theta = 123.4°$) was that used in Mc_4,4 (100% laser power and 40 μm pitch).

SEM observations support the previous data obtained by confocal microscopy. Fig. 6 shows some of the micrographs taken from the SEM analysis of the four stones before and after texturing with grooves and craters, both of surfaces and cross-sectional cuts.

First, SEM shows the different morphological starting points of the surfaces of each stone. Despite their polished finish, the untreated surfaces of slate and granite (Fig. 6a and c, respectively) possess significant irregularities related to their cleavage. The surface of the quartzite (Fig. 6b), despite being somewhat more homogeneous, is nonetheless affected by holes corresponding to the veins present in the stone. The marble (Fig. 6d) possesses a more homogeneous surface, on which a pattern of fissuring that matches the perfect rhombohedral cleavage of calcite grains is clearly present.

The observation of the textured surfaces (Fig. 6e–h) shows that the uniformity of the patterns (grooves and craters) on the surfaces of the slate, quartzite, and granite is very different from that observed on marble (Fig. 6h). On the first three stones, the continuity of grooves is not constant across the textured surface (Fig. 6e–g). On the contrary, on the marble (Fig. 6h), the uniformity of the pattern is much more constant across the entire textured surface: with the exception of areas containing fractures, the grooves are continuous almost along the entire line, and the crater pattern is also uniform and continuous.

Observing the cross-sectional cuts reveals a few differences. On one hand, the relief of the pattern is less uniform in the case of slate (Fig. 6i), quartzite (Fig. 6j), and granite (Fig. 6k). In these stones, the peaks and valleys have different dimensions and angles. In slate and granite, we observe that the mineralogy and texture contribute to this irregular pattern. Specifically, in granite, we observe certain melted biotite grains which smooth out the relief (Fig. 6k), while in slate the fine grain causes grains to stick out along the profile (Fig. 6i). In quartzite, the presence of transgranular fissures interrupts the uniformity of the pattern, as observed in the cross-sectional cut of this rock textured with craters (Fig. 6j). On the contrary, the textured pattern of marble is uniform: the peaks and valleys have similar dimensions and the edges of the stone are smooth and continuous (Figure 6l). Our observations indicate that the marble samples subjected to low laser power and high pitch conserved the stone's original surface (Figure 6m). We also observe that some marble samples textured at maximum laser power have a surface that presents peaks whose edges are likely signs of surface fusion (Figure 6n).

The transmitted light microscopy observations (Fig. 7) corroborate with the above observations. In the case of slate, quartzite, and marble (Fig. 7a, b, and d, respectively), transmitted light microscopy shows that all minerals are affected homogeneously because the depths of the valleys are similar for the entire textured area. In the granite, this technique shows that the laser produces more pronounced indentations in the surface when biotite crystals are present (Fig. 7c). These show an incipient 'burning' mark. The indentations are probably triggered by the pronounced foliation of the granite, as the laser was used against a perpendicular surface of the foliation, acting parallel to this foliation.

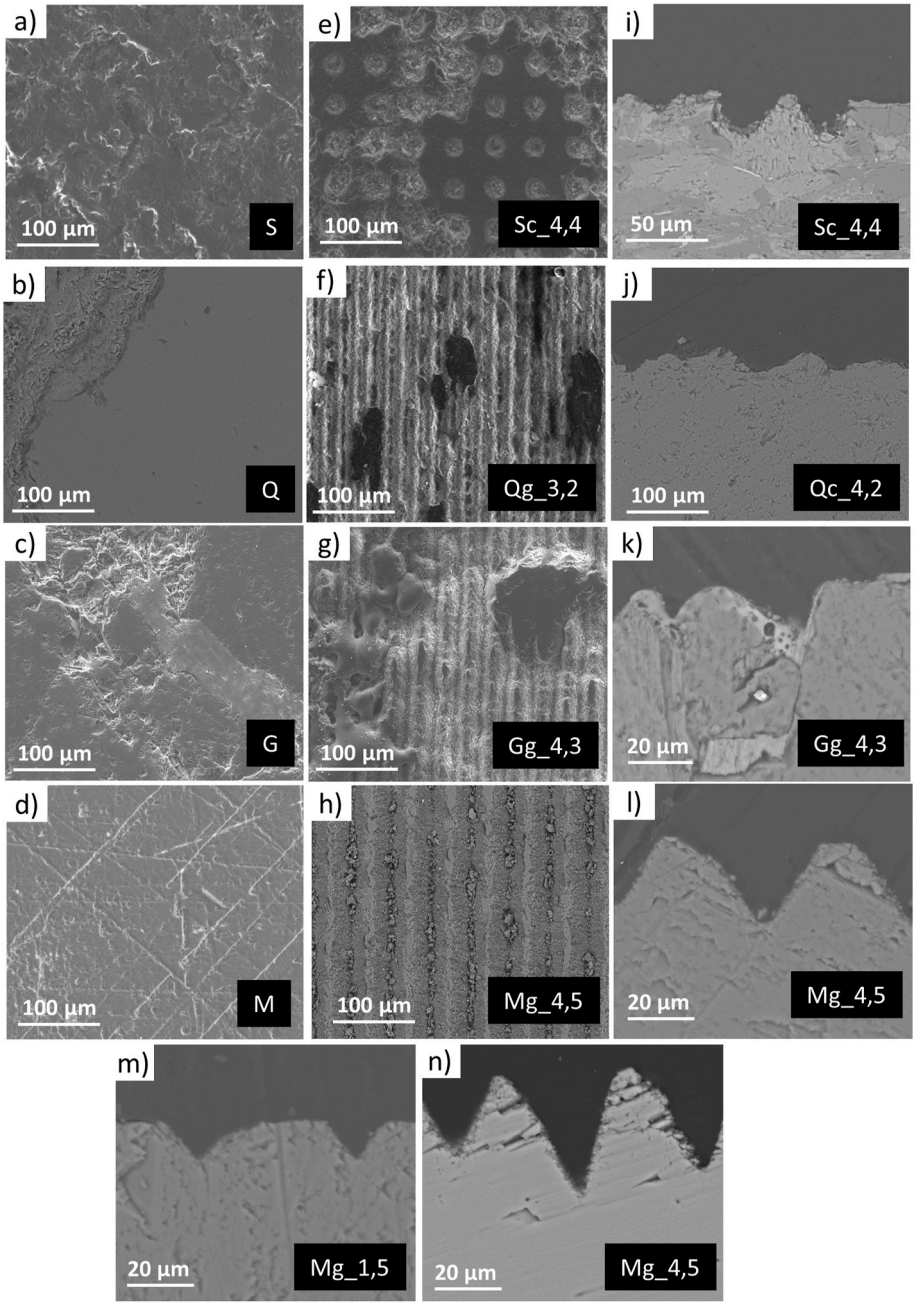

Fig. 6. SEM micrographs of the surfaces of the stones before (a: slate, b: quartzite, c: granite, and d: marble) and after texturing under different conditions (e–h). Moreover, the SEM micrographs of cross-sections are also shown (i–n).

4.3. Effects on stone colour

Fig. 8 shows the ΔE^*_{ab} after texturing the four stones under different conditions. In slate, both patterns (grooves and craters) induced visible changes in colour, since ΔE^*_{ab} exceeded the visual perception limit established as 3.5 CIELAB units [42]. In groove-textured surfaces, almost all treatments produced a ΔE^*_{ab} greater than 3.5 CIELAB units, except for the Sg_1,8 surface (Fig. 8a), which was the surface that presented the θ closest to the reference value. The results of the statistical analysis (Table 3) confirmed statistically significant regression relationships between power and ΔE^*_{ab} (positive: the greater the power, the larger the ΔE^*_{ab}) and between pitch and ΔE^*_{ab} (negative: the greater the distance, the smaller the ΔE^*_{ab}). In crater-textured samples, the number of laser texturing conditions that led to a ΔE^*_{ab} greater than 3.5 CIELAB units was notably lower. However, the ΔE^*_{ab} of the surfaces treated with the lowest pitch was greater compared to that obtained in groove-textured surfaces. The lowest ΔE^*_{ab} was obtained in surface Sc_1,8, the θ of which was the closest to the reference value. A strong statistically significant regression was obtained between the pitch

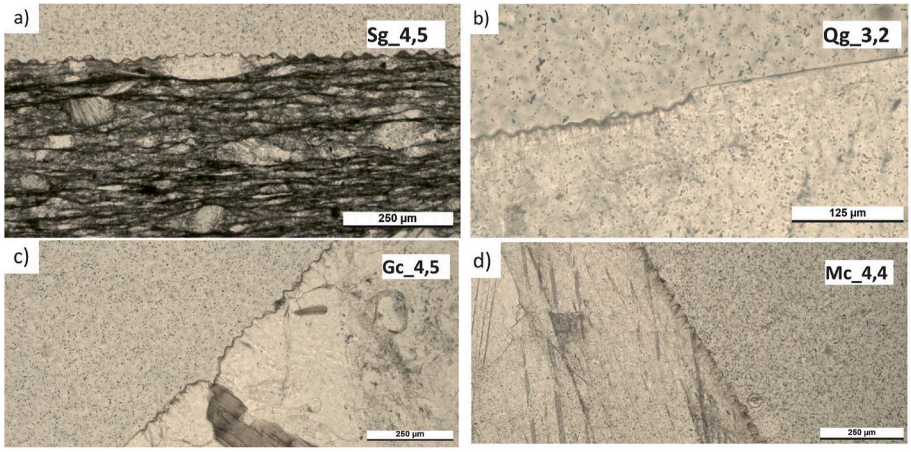

Fig. 7. Micrographs taken via polarized light microscopy of the thin sections of some of the samples irradiated at a higher power: a) slate, b) quartzite, d) granite, and d) marble.

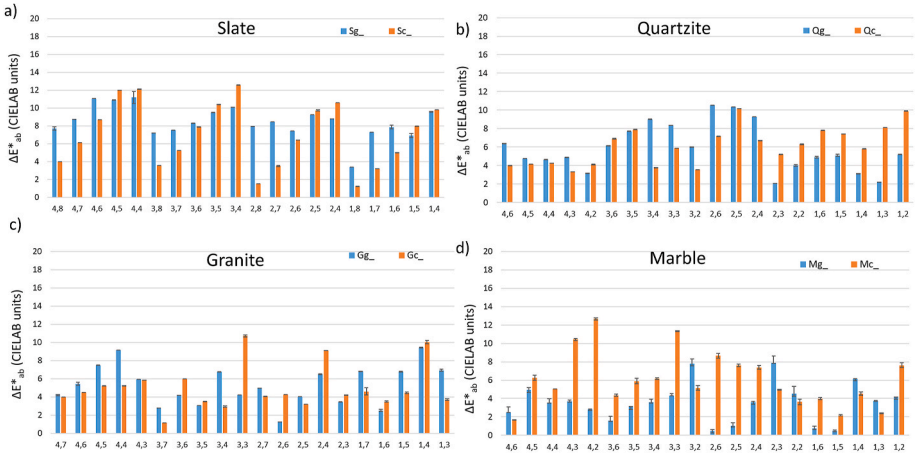

Fig. 8. ΔE*ab of the different textured areas: a) slate, b) quartzite, c) granite, and d) marble. Error bars length correspond to ± one standard deviation.

and ΔE^*_{ab} (negative: the greater the distance, the smaller the ΔE^*_{ab}).

In quartzite (Fig. 8b), ΔE^*_{ab} after laser texturing was not as high as in slate. In groove-textured surfaces, the areas that suffered from the greatest ΔE^*_{ab} were those textured at mid-range power levels (3.2 W and 2.4 W) and higher distances (60 µm, 50 µm, and 40 µm). As confirmed by the simple regression analysis (Table 3), there was a statistically significant relationship between the power and ΔE^*_{ab} (with a negative slope) and a less significant relationship between the pitch and ΔE^*_{ab} (with a positive slope). In crater-textured areas, ΔE^*_{ab} was somewhat lower than in groove-textured surfaces; the areas with the greatest ΔE^*_{ab} coincided with the areas processed at a lower power (unlike in slate and groove-textured quartzite) and at a smaller pitch. In this case, a statistically significant regression relationship was found between the power and ΔE^*_{ab}; however, as opposed to what happened in the case of slate, this relationship was inverse (the higher the power, the smaller the ΔE^*_{ab}).

In granite (Fig. 8c), as in the previous stones, laser texturing produced colour changes. However, ΔE^*_{ab} exceeded the visual perception limit in fewer cases than for slate and quartzite. There seems to be no relationship between ΔE^*_{ab} and the pitch or laser power, neither in groove-textured areas nor in crater-textured areas.

The colour change in the marble (Fig. 8d) after texturing was not as noticeable as that observed in the other three stones: ΔE^*_{ab} exceeded the visual perception limit in fewer cases than for slate and quartzite. In groove-textured areas, no relationship between ΔE^*_{ab} and the power was detected (Table 3). In fact, the statistical analysis only detected a statistically significant relationship between the pitch and ΔE^*_{ab}, which had a negative slope. In the area in which the highest θ was achieved (Mg_4,5, with a value of $\theta = 127.47°$), ΔE^*_{ab} was slightly greater than 4 CIELAB units (thus exceeding the visual perception limit), but was not the highest ΔE^*_{ab} value. In fact, the statistical analysis ruled out the existence of a correlation between θ and ΔE^*_{ab}.

In crater-textured marble (Fig. 8d), ΔE^*_{ab} was higher than that recorded in groove-textured surfaces. No statistically significant relationship was obtained between ΔE^*_{ab} and the power or pitch (Table 3). In the surface with the highest θ (Mc_4,4, with a value of $\theta = 123.39°$), ΔE^*_{ab} exceeded the limit of visual perception but its value (slightly greater than 4 CIELAB units) was not one of the highest

(note that the highest value of ΔE^*_{ab} in these cases was 12 CIELAB units).

Supplementary Data S2 S2 includes the values of the different colour parameters measured (L*, a*, b*, C^*_{ab}, and h_{ab}) and their differences compared to the colour of the reference surface prior to the texturing.

5. Discussion

To determine if the stones' wettability changed and the extent to which this change can be attributed to laser texturing, we conducted a correlation analysis of the variables characterising the Wenzel (Eq. (1)) and Cassie-Baxter (Eq. (2)) regimes, and specifically the cosine of the contact angle $cos\theta$ and the surface roughness parameters characterising the texture of each of the stones analysed.

Table 4 shows the p and of R^2 values (in parentheses) of the simple regression analysis of the cosine of the contact angle cos and the variables z_p (the depth of the texture) and surface roughness S_{dr} (the developed interfacial area ratio). As a global variable, the colour change ΔE^*_{ab} was also included.

The results shown in Table 4 demonstrate that there is a statistically significant correlation between $cos\theta$ and the depth of the texture pattern z_p for all cases except for slate containing craters. Furthermore, the slope is positive for slate and quartzite and negative for marble. A similar behaviour is found for S_{dr}, but the craters in the marble are not significant in this case. The sign of the slope indicates the wettability behaviour of the rock surface: a positive slope corresponds to a Wenzel regime (i.e., total penetration of the liquid into surface grooves) and a negative slope corresponds to the Cassie-Baxter regime (in which microscopic pockets of air remain trapped below the liquid droplet). In other words, in granite and quartzite, an increase in the parameters z_p and S_{dr} and, therefore, in the surface area of the solid in contact with the liquid is accompanied by a decrease in the contact angle with respect to the polished surface. However, the opposite occurs in marble.

Regarding colour changes, Table 4 shows the existence of a statistically significant correlation between $cos\theta$ and ΔE^*_{ab} for slate and quartzite, but which is not statistically significant for marble. Nonetheless, in the case of slate and quartzite, the slope has a different sign, as it is positive in the case of slate and negative in the case of quartzite.

In the case of slate, laser texturing results in an intense colour change (the stone becomes lighter) reflected in its ΔE^*_{ab} value. The laser eliminates the polish, and as a result, the shine and black colour accompanying it, with the laser texturing on the surface also being visible to the naked eye (Fig. 1g and h). In this stone, a smaller contact angle and therefore a greater S_{dr} results in a higher ΔE^*_{ab} value. However, in quartzite, an increase in the texturing does not result in an increase in ΔE^*_{ab}. Visually speaking, the effect of laser texturing on the appearance of this stone is not as apparent as in the case of slate. In the case of textured marble, independent of the values of the different parameters, there is no effect on ΔE^*_{ab}. Moreover, visually speaking, the colour change is almost imperceptible (Fig. 1k and l).

These differences in terms of the stones' colour change following laser processing may be related to the mineralogical composition of the stones and their texture, as both of these aspects determine a stone's colour with and without polishing and following laser texturing (although in the latter case, a third variable is involved, specifically the reaction of the component minerals to laser irradiation). Slate is very fine-grained and has a characteristic black colour. Polishing intensifies its black colour but texturing causes a very notable increase in its lightness (in other words, its surface becomes lighter). Specifically, the colorimetric component that changes the most following texturing is the coordinate L* (see supplementary data). This increase in L* can be explained by the effects of one of slate's main components on its appearance, namely its muscovite-sericite content. Therefore, eliminating polishing via texturing would return slate's characteristic shine, which is conferred by small particles of sericite-muscovite. In granite, the overall colour change is due to changes in the L* coordinate but also the a* and b* coordinates. As a result, out of the parameters of colour, lightness, chroma (colour intensity), and hue (tone), three were modified: granite's larger grain size combined with the modification undergone by the darkest mineral (biotite, which undergoes fusion) and the impact on the iron oxyhydroxides that fill in the cracks in this stone (which have an impact on colour following laser irradiation as confirmed in previous research [43]) are the three factors that explain the colour change in granite following texturing. In quartzite and marble, the greatest impact of the texturing on colour is produced in the L* coordinate (see supplementary data). This is because the laser eliminates the initial shine, which (due to the monomineralic nature and very low porosity of these two stones compared to the other two) is already initially very high.

On the other hand, with respect to the laser's effects on the different minerals (in the case of granite, quartz, biotite, and k-feldspar are the major minerals), the SEM micrographs obtained show that they have different responses to laser processing, resulting in different morphologies that can be attributed, among other reasons, to the effect of heat accumulation induced by high-repetition pulses [44,45]. This phenomenon is strongly influenced by material properties (thermal diffusivity, reflectivity) and processing parameters (laser fluence, temporal and spatial displacement). In this sense, the residual laser energy absorbed that did not contribute to the ablation process remains, leading to different effects, such as the formation of a thin layer of melt phase [46]. In this sense, this research once again confirms that out of the minerals composing the silicate rocks studied, biotite is that most susceptible to alteration due to laser irradiation, as its breakdown becomes more intense as the laser power increases and as the distance between the grooves and/or craters decreases. Previous research has already observed this greater susceptibility by applying nanosecond lasers [47]. In this case, the biotite's greater susceptibility was attributed to its lower fusion temperature. In the case of ultrashort pulse lasers, previous research using a femtosecond laser with 120 fs pulses at 790 with a repetition rate of 1 kHz [29], confirmed mineral alterations in granite, although they were much less intensive and more selective, which may show that deterioration with ultrashort short pulse lasers reduces the thermal impact.

The polymineralic nature of granite and slate may cause the texturing pattern on the surface of the rock to be irregular, which will affect hydrophobicity. Nonetheless, this polymineralic nature is not the only textural parameter of the stones that makes it difficult to

Table 4
p and R^2 (in parentheses) values of the simple regression analysis of the cosine of the contact angle $cos\theta$ and the variables z_p (depth of the texture fit), surface roughness S_{dr} (developed interfacial area ratio), and global colour change ΔE^*_{ab}, for each of the stones (S: slate, Q: quartzite, M: marble) textured with grooves (Sg, Qg and Mg) and craters (Sc, Qc and Mc). Statistically, non-significant regression relationships ($p > 0.05$) have been replaced by a hyphen.

$cos\theta$	Correlation Analysis		
Sample	z_p	S_{dr}	ΔE^*_{ab}
S-g	0.04 (0.46)	7.9e-05 (0.77)	6.5e-07 (0.87)
S-c	–	9.6e-05 (0.76)	1.1e-09 (0.94)
Q-g	0.0067 (0.59)	0.0011 (0.68)	1.5e-07 (−0.89)
Q-c	1.5e-05 (0.96)	0.026 (0.69)	3.4e-05 (−0.79)
M-g	0.039 (−0.46)	0.011 (−0.56)	–
M-c	0.0077 (−0.58)	–	–

obtain uniform texturing. For example, we observe that the pattern on quartzite is much less uniform than on marble, despite the fact that both rocks are monomineralic and start with a similar initial polish (with the initial roughness of quartzite even being slightly less than that of marble). The irregularity of the pattern on quartzite may be related to the grain size: in marble, calcite has a grain size of around 500 μm, whereas the size of the quartz grains in quartzite is highly heterometric (crystals with sizes varying between 500 μm and 30 μm are observed). This difference in grain size is why the negative effects of transgranular fissuring on the uniformity of the pattern are much greater in quartzite than in marble.

Lastly, Table 5 contains the conditions under which the highest and lowest θ values were obtained in each stone, as well as the corresponding z_p, S_{dr}, and ΔE^*_{ab} values. We observe that in slate, quartzite, and granite the maximum contact angle values (which are never greater than 90°) and the minimum values always decrease compared to the reference value, with the greatest reduction in θ in comparison to the reference value occurring at maximum laser power values, and in almost all cases, at the smallest pitch. We also see that the greatest reductions in contact angle values occur with the highest z_p and S_{dr} values. As stated, all of this is in line with behaviour under the Wenzel regime, in which an increase in S_{dr} and, therefore, in the surface of the solid in contact with the liquid is accompanied by a decrease in the contact angle compared to the polished surface. In the case of marble, the opposite happens, with the maximum/minimum contact angle values corresponding to the highest/lowest values in the parameter S_{dr} in accordance with the Cassie-Baxter model. In this stone, the largest θ values are obtained at the highest powers applied and the smallest θ values are produced at lower powers. The influence of the pitch is small, except in the case of 20 μm, which corresponds to a separation that is smaller than the laser spot size, thus causing the partial destruction of the texturing due to the laser's effects on neighbouring areas. This effect is mainly noted at high powers.

As stated above, it is necessary to keep in mind that marble starts with a surface with less localised irregularities than the other stones and with a contact angle that is already very close to 90°. As a result, as implicated by the Cassie-Baxter model (Eq. (2)), it is more feasible for the texturing to produce an increase in the contact angle, obtaining values that oscillate between 123° and 127°, thus increasing the hydrophobicity of the stone.

An important aspect to note in an analysis of the behaviour of the different stones when subjected to laser texturing, as mentioned in the above paragraph, is the effects of the surface irregularities that persist in the stones used despite polishing, which exist on a much larger scale than the dimensions of the texturing. These irregularities, which in some cases are measured on scales that are much larger than micrometres, compromise the continuity and periodicity of the laser-generated patterns and therefore the potential effects that this treatment may have on the stone's wettability.

Table 5
Laser power and pitch conditions under which the highest and lowest θ values were obtained. The z_p, S_{dr}, and ΔE^*ab parameters of the laser-textured areas (treated with either grooves or craters) and the increase in the contact angle $\Delta\theta$ are also shown. Statistically, non-significant values have been replaced by a hyphen.

ID	Power [W]	Pitch [μm]	θ° [Δθ°]	z_p [μm]	S_{dr}[μm]	ΔE^*_{ab}
Sg_1,8	1.6	80 (max)	56.61 ± 6.94 (−16.8°)	4.95 ± 0.11	0.081	3.38
Sg_4,5	4	50 (min)	18.66 ± 9.97 (- 54.7°)	10.22 ± 0.17	0.208	10.88
Sc_2,8	2.4	80 (max)	44.01 ± 7.30 (−29.4°)	16.64 ± 0.08	0.137	1.52
Sc_4,4	4	40 (min)	18.37 ± 9.25 (−55.0°)	19.41 ± 0.1	0.48	12.12
Qg_1,6	1.6	60 (max)	56.61 ± 10.75 (−13.11°)	1.07 ± 0.04	0.016	5
Qg_3,2	3.2	20 (min)	10.84 ± 0.66 (−58.8°)	1.98 ± 0.33	0.057	5.97
Qc_1,6	1.6	60 (max)	68.45 ± 1.35 (−1.3°)	–	–	7.9
Qc_4,2	4	20 (min)	13.04 ± 3.25 (−56.8°)	–	–	4.1
Gg_1,7	1.6	70 (max)	22.34 ± 0.22 (−21.6°)	2.4 ± 154.95	0.065	6.81
Gg_4,3	4	30 (min)	0	11.75 ± 0.63	0.445	5.93
Gc_1,6	1.6	60 (max)	40.20 ± 0.20 (−3.3°)	10.03 ± 0.07	0.047	3.5
Gc_4,5	4	50 (min)	0	22.67 ± 0.11	0.25	5.21
Mg_4,5	4	50 (max)	127.47 ± 7.00 (61.1°)	18.96 ± 0.14	0.591	4.94
Mg_1,5	1.6	50 (min)	62.50 ± 15.15 (−3.8°)	7.63 ± 0.08	0.133	0.48
Mc_4,4	4	40 (max)	123.39 ± 23.18 (57.1°)	24.78 ± 0.1	0.487	5.05
Mc_1,4	1.6	40 (min)	83.71 ± 1.07 (17.4°)	4.21 ± 0.03	0.056	4.53

Conclusions

In this research, for the first time, the modifications by femtosecond laser structuring of the wetting properties of four ornamental rocks with different lithologies and textural characteristics (marble, quartzite, granite and slate) were investigated. The results obtained using similar texturing patterns show a correlation statistically significant between the change in the contact angle θ, which characterizes the wettability of the stone, and the generated surface roughness; so that, in the group composed of slate, quartzite, and granite laser texturing caused a decrease in the contact angle and, therefore, made the surface even more receptive to water compared to the polished one; on the contrary, laser texturing was able to increase the contact angle of marble up to values $\theta_{marble} \approx 125^{\circ}$ thus giving a clear hydrophobic behaviour to the stone surface. These changes in contact angle are also correlated with colour change in the group composed of slate, quartzite, and granite; while in the case of marble no correlation is observed, and in addition, the texturing effects are barely perceptible visually in this rock.

From this research, it was also concluded that despite of the polished finish of the rock surfaces, the grain size and other petrographic features, such as type of fissures affect the continuity and uniformity of structuring patterns and, consequently, the success of this technique as a method to waterproof ornamental stones. In any event, the successful results obtained with marble leave open new possibility with other stones, which will require a particular study in each case. Finally, further investigation must be accomplished to analyse the temporal evolution of the wetting characteristics of the surface, and the mechanisms (chemical or mineralogical) involved, to increase the hydrophobicity of marble up to super-hydrophobic levels.

CRediT authorship contribution statement

A.J. López: Conceptualization, Methodology, Investigation, Formal analysis, Resources, Writing – review & editing. **J.S. Pozo-Antonio:** Methodology, Investigation, Formal analysis, Writing – original draft. **A. Moreno:** Investigation, Software, Formal analysis, Resources. **T. Rivas:** Conceptualization, Methodology, Investigation, Resources, Writing – review & editing. **D. Pereira:** Methodology, Investigation, Formal analysis, Resources. **A. Ramil:** Conceptualization, Methodology, Investigation, Software, Formal analysis, Resources, Data curation, Funding.

Declaration of competing interest

The authors declare that they have no known competing financial interests or personal relationships that could have appeared to influence the work reported in this paper.

Acknowledgements

This research was funded by the Spanish Ministerio de Economía y Competitividad under grant number BIA2017-85897-R. J.S. Pozo-Antonio was financed by the University of Vigo through a contract as Distinguished Researcher. MD Pereira had access to the ICP-MS and XRD thanks to the University of Salamanca research centre. We thank Diego Sanromán for his technical assistance.

Appendix A. Supplementary data

Supplementary data to this article can be found online at https://doi.org/10.1016/j.jobe.2022.104176.

References

[1] A.E. Charola, Water-repellent treatments for building stones: a practical overview, APT Bull. 26 (1995) 10, https://doi.org/10.2307/1504480.
[2] T. Warscheid, J. Braams, Biodeterioration of stone: a review, Int. Biodeterior. Biodegrad. 46 (2000) 343–368, https://doi.org/10.1016/S0964-8305(00)00109-8.
[3] B. Cámara, M.Á. de Buergo, M. Bethencourt, T. Fernández-Montblanc, M.F. La Russa, M. Ricca, R. Fort, Biodeterioration of marble in an underwater environment, Sci. Total Environ. 609 (2017) 109–122, https://doi.org/10.1016/J.SCITOTENV.2017.07.103.
[4] M. Aldoasri, S. Darwish, M. Adam, N. Elmarzugi, S. Ahmed, M.A. Aldoasri, S.S. Darwish, M.A. Adam, N.A. Elmarzugi, S.M. Ahmed, Enhancing the durability of calcareous stone monuments of ancient Egypt using CaCO3 nanoparticles, Sustainability 9 (2017) 1392, https://doi.org/10.3390/su9081392.
[5] R. Zarzuela, I. Moreno-Garrido, J. Blasco, M.L.A. Gil, M.J. Mosquera, Evaluation of the effectiveness of CuONPs/SiO2-based treatments for building stones against the growth of phototrophic microorganisms, Construct. Build. Mater. 187 (2018) 501–509, https://doi.org/10.1016/J.CONBUILDMAT.2018.07.116.
[6] P.N. Manoudis, A. Tsakalof, I. Karapanagiotis, I. Zuburtikudis, C. Panayiotou, Fabrication of super-hydrophobic surfaces for enhanced stone protection, Surf. Coating. Technol. 203 (2009) 1322–1328, https://doi.org/10.1016/J.SURFCOAT.2008.10.041.
[7] M. Sadat-Shojai, A. Ershad-Langroudi, Polymeric coatings for protection of historic monuments: Opportunities and challenges, J. Appl. Polym. Sci. 112 (2009) 2535–2551, https://doi.org/10.1002/app.29801.
[8] S. Andreotti, E. Franzoni, P. Fabbri, P. Fabbri, Poly(hydroxyalkanoate)s-Based hydrophobic coatings for the protection of stone in cultural heritage, Materials 2018 11 (165) (2018) 11–165, https://doi.org/10.3390/MA11010165.
[9] J. Bico, U. Thiele, D. Quéré, Wetting of textured surfaces, Colloids Surf. A Physicochem. Eng. Asp. 206 (2002) 41–46, https://doi.org/10.1016/S0927-7757(02)00061-4.
[10] M. Nosonovsky, B. Bhushan, Biologically inspired surfaces: broadening the scope of roughness**, Adv. Funct. Mater. 18 (2008) 843–855, https://doi.org/10.1002/adfm.200701195.
[11] L. Gao, T.J. McCarthy, The “lotus effect” explained: two reasons why two length scales of topography are important, Langmuir 22 (2006) 2966–2967, https://doi.org/10.1021/LA0532149/SUPPL_FILE/LA0532149_S.PDF.
[12] T. Darmanin, F. Guittard, Superhydrophobic and superoleophobic properties in nature, Mater. Today 18 (2015) 273–285, https://doi.org/10.1016/J.MATTOD.2015.01.001.

[13] L. Feng, S. Li, Y. Li, H. Li, L. Zhang, J. Zhai, Y. Song, B. Liu, L. Jiang, D. Zhu, Super-hydrophobic surfaces: from natural to artificial, Adv. Mater. 14 (2002) 1857–1860, https://doi.org/10.1002/adma.200290020.
[14] A. Tsakalof, P. Manoudis, I. Karapanagiotis, I. Chryssoulakis, C. Panayiotou, Assessment of synthetic polymeric coatings for the protection and preservation of stone monuments, J. Cult. Herit. 8 (2007) 69–72, https://doi.org/10.1016/J.CULHER.2006.06.007.
[15] G. Cappelletti, P. Fermo, Hydrophobic and superhydrophobic coatings for limestone and marble conservation, in: Smart Composite Coatings and Membranes, Elsevier, 2016, pp. 421–452, https://doi.org/10.1016/B978-1-78242-283-9.00015-4.
[16] J.F. Illescas, M.J. Mosquera, Surfactant-synthesized PDMS/silica nanomaterials improve robustness and stain resistance of carbonate stone, J. Phys. Chem. C 115 (2011) 14624–14634, https://doi.org/10.1021/JP203524P/SUPPL_FILE/JP203524P_SI_001.PDF.
[17] D.S. Facio, M.J. Mosquera, Simple strategy for producing superhydrophobic nanocomposite coatings in situ on a building substrate, ACS Appl. Mater. Interfaces 5 (2013) 7517–7526, https://doi.org/10.1021/AM401826G.
[18] J.D. Rodrigues, A. Grossi, Indicators and ratings for the compatibility assessment of conservation actions, J. Cult. Herit. 8 (2007) 32–43, https://doi.org/10.1016/J.CULHER.2006.04.007.
[19] S. Sarbada, Y.C. Shin, Superhydrophobic contoured surfaces created on metal and polymer using a femtosecond laser, Appl. Surf. Sci. 405 (2017) 465–475, https://doi.org/10.1016/J.APSUSC.2017.02.019.
[20] D. Huerta-Murillo, A. García-Girón, J.M. Romano, J.T. Cardoso, F. Cordovilla, M. Walker, S.S. Dimov, J.L. Ocaña, Wettability modification of laser-fabricated hierarchical surface structures in Ti-6Al-4V titanium alloy, Appl. Surf. Sci. 463 (2019) 838–846, https://doi.org/10.1016/J.APSUSC.2018.09.012.
[21] E. Fadeeva, B. Chichkov, Biomimetic Liquid-Repellent Surfaces by Ultrafast Laser Processing, (n.d.). https://doi.org/10.3390/app8091424.
[22] A.O. Ijaola, E.A. Bamidele, C.J. Akisin, I.T. Bello, A.T. Oyatobo, A. Abdulkareem, P.K. Farayibi, E. Asmatulu, Wettability transition for laser textured surfaces: a comprehensive review, Surface. Interfac. 21 (2020) 100802, https://doi.org/10.1016/J.SURFIN.2020.100802.
[23] C. Kunz, F.A. Müller, S. Gräf, Multifunctional hierarchical surface structures by femtosecond laser processing, Materials 11 (2018) 789, https://doi.org/10.3390/MA11050789, 11 (2018) 789.
[24] A. Chantada, J. Penide, P. Pou, A. Riveiro, J. del Val, F. Quintero, R. Soto, F. Lusquiños, J. Pou, Laser surface texturing of granite, Procedia Manuf. 13 (2017) 687–693, https://doi.org/10.1016/J.PROMFG.2017.09.144.
[25] A. Chantada, J. Penide, A. Riveiro, J. del Val, F. Quintero, M. Meixus, R. Soto, F. Lusquiños, J. Pou, Increasing the hydrophobicity degree of stonework by means of laser surface texturing: an application on Zimbabwe black granites, Appl. Surf. Sci. 418 (2017) 463–471, https://doi.org/10.1016/J.APSUSC.2016.12.196.
[26] A.J. López, A. Ramil, J.S. Pozo-Antonio, T. Rivas, D. Pereira, Ultrafast laser surface texturing: a sustainable tool to modify wettability properties of marble, Sustainability 11 (2019) 4079, https://doi.org/10.3390/su11154079.
[27] R. Ariza, M. Alvarez-Alegria, G. Costas, L. Tribaldo, A.R. Gonzalez-Elipe, J. Siegel, J. Solis, Multiscale ultrafast laser texturing of marble for reduced surface wetting, Appl. Surf. Sci. 577 (2022) 151850, https://doi.org/10.1016/j.apsusc.2021.151850.
[28] R. Stoian, J.-P. Colombier, Advances in ultrafast laser structuring of materials at the nanoscale, Nanophotonics 9 (2020) 4665–4688, https://doi.org/10.1515/NANOPH-2020-0310.
[29] T. Rivas, A.J. Lopez, A. Ramil, S. Pozo, M.P. Fiorucci, M.E.L. De Silanes, A. García, J.R.V. De Aldana, C. Romero, P. Moreno, Comparative study of ornamental granite cleaning using femtosecond and nanosecond pulsed lasers, Appl. Surf. Sci. 278 (2013) 226–233, https://doi.org/10.1016/J.APSUSC.2012.12.038.
[30] P.G. de Gennes, Wetting: statics and dynamics, Rev. Mod. Phys. 57 (1985) 827–863, https://doi.org/10.1103/RevModPhys.57.827.
[31] K.M. Al Balushi, K. Sefiane, D. Orejon, Binary mixture droplet wetting on micro-structure decorated surfaces, J. Colloid Interface Sci. 612 (2022) 792–805, https://doi.org/10.1016/J.JCIS.2021.12.171.
[32] A. Marmur, Wetting on hydrophobic rough surfaces: to Be heterogeneous or not to Be?. https://doi.org/10.1021/la0344682, 2003.
[33] Igme, Mapa Geológico de España E1:50.000, Serie magna (2ªEdición), Hoja 190, El Barco de Valdeorras, Madird, 1981.
[34] CEN, EN 1936:2006. Natural Stone Test Methods - Determination of Real Density and Apparent Density, and of Total and Open Porosity, 2006. Luxembourg.
[35] Igme, Mapa Geológico de España E 1:50000, Serie Magna (2ªEdición), Hoja 261, Tui, Servicio de Publicaciones Del Ministerio de Industria y Energía, 1981.
[36] ASTM International, ASTM C1721 - 15 standard guide for petrographic examination of dimension stone. https://www.astm.org/Standards/C1721.htm, 2015.
[37] AENOR, UNE-EN 828: 2013, Adhesives - Wettability - Determination by Measurement of Contact Angle and surface Free Energy of solid surface, 2013. Madrid.
[38] AENOR, UNE-EN ISO 25178-2:2013, Geometrical Product specifications (GPS) — Surface Texture: Areal —Part 2: Terms, Definitions and surface Texture Parameters, 2013. Madrid.
[39] M.P. Fiorucci, A.J. López, A. Ramil, Multi-scale characterization of topographic modifications on metallic biomaterials induced by nanosecond Nd:YVO4 laser structuring, Precis. Eng. 53 (2018) 163–168, https://doi.org/10.1016/J.PRECISIONENG.2018.03.009.
[40] CIE, S014-4:2007, Colorimetry—Part 4: CIE 1976 L*a*b*, Colour Space, Vienna, 2007.
[41] M.J. Mosquera, T. Rivas, B. Prieto, B. Silva, Capillary rise in granitic rocks: interpretation of kinetics on the basis of pore structure, J. Colloid Interface Sci. 222 (2000) 41–45, https://doi.org/10.1006/JCIS.1999.6612.
[42] W. Mokrzycki, M. Tatol, Color difference Delta E-A survey, Mach. Graph. and Vis. 20. 4 (2011).
[43] T. Rivas, J.S. Pozo-Antonio, A. Ramil, A.J. López, Influence of the weathering rate on the response of granite to nanosecond UV laser irradiation, Sci. Total Environ. 706 (2020) 135999, https://doi.org/10.1016/J.SCITOTENV.2019.135999.
[44] E. Saavedra, A.J. López, J. Lamas, M.P. Fiorucci, A. Ramil, T. Rivas, Finite element model of granite ablation with UV laser, Mater. Sci. Forum 730–732 (2013) 519–524, https://doi.org/10.4028/WWW.SCIENTIFIC.NET/MSF.730-732.519.
[45] F. Bauer, A. Michalowski, T. Kiedrowski, S. Nolte, Heat accumulation in ultra-short pulsed scanning laser ablation of metals, Opt Express 23 (2015) 1035, https://doi.org/10.1364/OE.23.001035.
[46] Y. Hirayama, M. Obara, Heat effects of metals ablated with femtosecond laser pulses, Appl. Surf. Sci. 197–198 (2002) 741–745, https://doi.org/10.1016/S0169-4332(02)00403-8.
[47] A. Ramil, J.S. Pozo-Antonio, M.P. Fiorucci, A.J. López, T. Rivas, Detection of the optimal laser fluence ranges to clean graffiti on silicates, Construct. Build. Mater. 148 (2017) 122–130, https://doi.org/10.1016/J.CONBUILDMAT.2017.05.035.